

SOCRATES: A Stereo Camera Trap for Monitoring of Biodiversity

Timm Haucke^a, Hjalmar Kühl^b, Volker Steinhage^a

^aUniversity of Bonn, Institute of Computer Science IV, Friedrich-Hirzebruch-Allee 8, Bonn 53115, Germany

^bMax Planck Institute for Evolutionary Anthropology, Department of Primatology, Deutscher Platz 6, Leipzig 04103, Germany

Abstract

The development and application of modern technology is an essential basis for the efficient monitoring of species in natural habitats and landscapes to trace the development of ecosystems, species communities, and populations, and to analyze reasons of changes. For estimating animal abundance using methods such as camera trap distance sampling, spatial information of natural habitats in terms of 3D (three-dimensional) measurements is crucial. Additionally, 3D information improves the accuracy of animal detection using camera trapping. This study presents a novel approach to 3D camera trapping featuring highly optimized hardware and software. This approach employs stereo vision to infer 3D information of natural habitats and is designated as **StereO CameRA Trap** for monitoring of biodiversi**Er**Sity (SOCRATES). A comprehensive evaluation of SOCRATES shows not only a 3.23% improvement in animal detection (bounding box mAP₇₅) but also its superior applicability for estimating animal abundance using camera trap distance sampling. The software and documentation of SOCRATES is provided at <https://github.com/timmh/socrates>.

Keywords: stereo vision, camera trapping, animal density, animal abundance, instance segmentation

Email addresses: haucke@cs.uni-bonn.de (Timm Haucke), kuehl@eva.mpg.de (Hjalmar Kühl), steinhage@cs.uni-bonn.de (Volker Steinhage)

© 2022. This manuscript version is made available under the CC-BY-NC-ND 4.0 license <https://creativecommons.org/licenses/by-nc-nd/4.0/>

1. Introduction

The utilization of modern technology is commonplace in large-scale commercial, civil and strategic projects. But terrestrial ecology, in particular, is less well equipped. The potential of modern sensors, remote sensing, automated laboratory procedures, and complex data processing is hardly utilized at all within this field. This absence is one important reason why large-scale and long-term automated monitoring of biodiversity (as established for climate research) does not exist.

1.1. AMMODs Framework

To foster the adaption of modern technologies for the development of automated, reliable, and verifiable biodiversity monitoring, a network of **A**utomated **M**ultisensor stations for **M**onitoring of species **D**iversity (AMMODs) is proposed by Wägele et al. (2022) to pave the way for a new generation of biodiversity assessment stations. The AMMODs network approach combines cutting-edge technologies with biodiversity informatics and expert systems to conserve expert knowledge. The sensors employed in AMMODs range from traps for DNA barcoding over camera traps for visual monitoring, bioacoustics, to plant volatile compound detectors. The overall concept, the hardware and software components and the setup of AMMODs are described by Wägele et al. (2022). Within the AMMOD project, SOCRATES is specifically concerned with the visual monitoring of wildlife. SOCRATES derives and utilizes depth information as a third dimension in addition to the regular two dimensions (i.e., height and width pixel coordinates) of conventional camera trap images.¹

1.2. SOCRATES Contributions

- **Detection and localization of animals** in camera trap images are often unreliable. The additional depth information provided by SOCRATES fosters the accuracy and reliability of visual animal detection and animal localization within the monitored natural habitat.
- **Abundance estimation**, using methods such as camera trap distance sampling (CTDS), is traditionally performed using a combination of commercial camera trap hardware and very laborious manual workflows. SOCRATES instead provides depth information in a **fully automated** way using stereo vision.
- **Reproducibility and accessibility** for practitioners. This study report on SOCRATES takes the practitioner’s perspective and provides detailed setup and operational instructions.

¹In this contribution, the term *depth* refers to the distance between the camera trap and the observed animals.

1.3. Related Work

Related work is reported using two perspectives. First, recent progress with respect to visual object detection in images and video clips is reported. Second, an overview on approaches to estimate the density and abundance of unmarked animal populations using camera traps is given.

1.4. Visual Animal Detection

State-of-the-art approaches to visual animal detection utilize 2D deep learning object detection methods. Given a 2D color or grayscale image, these methods learn to predict a set of bounding boxes, e.g. given by the 2D location of the upper-left and bottom-right corner of an axis-aligned rectangle fully enclosing the animal. Object detection methods might be extended to perform *instance segmentation*, where not only bounding boxes are predicted, but whether any pixel in the image belongs to the respective object (binary masks). Deep learning object detection and instance segmentation models usually consist of two parts. The backbone takes in the original image and produces a hierarchy of *feature maps* that encode higher- and higher-level information about the image. These feature maps are then used by the object detection or instance segmentation model to predict the bounding boxes and binary masks themselves. A general issue of deep learning models is that their training requires immense amounts of *annotated* training data. Annotated data is raw data associated with corresponding labels, which can be of different modalities (e.g. object classes occurring in the image, bounding boxes around objects of interest, pixel-wise masks of such objects, etc.). These labels must often be created manually and are therefore costly to obtain. This requirement of large annotated training datasets is slightly relaxed by transfer learning. In transfer learning, the backbone is first pre-trained to perform some task involving a very large training dataset, e.g. performing image classification on ImageNet (Deng et al., 2009). Visual concepts learned by such backbones have been shown to be generally useful and not just applicable to the pre-training task (Zeiler and Fergus, 2014). The backbone is then fine-tuned on the target task, which usually involves a much smaller dataset.

1.4.1. Abundance Estimation

There exist a number of methods to estimate the density and abundance of unmarked animal populations using camera traps, e.g. the random encounter model (REM) (Rowcliffe et al., 2008), the random encounter and staying time model (REST) (Nakashima et al., 2018), the time-to-event model (TTE), space-to-event model (STE), instantaneous estimator (IS) (Moeller et al., 2018) and camera trap distance sampling (Howe et al., 2017). All of these require an estimation of the effective area surveyed by the camera trap. This area is not simply given by the optical constraints of the camera, instead it is influenced by factors such as environmental occlusion and the range of the passive infrared sensor. The effective area is statistically inferred by using the distances of the observed animals. Although there are approaches that estimate these distances



Figure 1: Introducing the SOCRATES camera trap system located in the wildlife park Plittersdorf located in Bonn, Germany, showing European fallow deer (*Dama dama*) and Sika deer (*Cervus nippon*).

(semi) automatically (Haucke et al., 2022; Johanns et al., 2022), they either require laborious capture of reference material (Haucke et al., 2022) or might not generalize to extreme scenarios such as very close-up scenes (Johanns et al., 2022; Auda, 2022).

2. Methods & Data

2.1. The SOCRATES Stereovision Sensor Platform

The SOCRATES camera trap system comprises a cost and power efficient stereovision sensor platform as well as state-of-the-art animal detection software based on a deep learning software architecture. The experimental evaluation of SOCRATES will utilize a representative RGB-D dataset generated by SOCRATES in the wildlife park Plittersdorf located in Bonn, Germany, showing fallow deer.

The central goal of SOCRATES is to infer depth information. Computer stereovision is the well-established approach to image-based depth estimation. By comparing information about an observed scene from two differing camera perspectives depth information can be derived. Mostly, both cameras in a stereo setup are displaced horizontally from one another yielding scene observations in terms of a left image and a right images. Computer stereo vision can be seen as the technical analogue to human stereopsis, that is, human perception of depth and three-dimensional structure by combining visual information from two eyes.

2.1.1. Depth by Stereovision

Depth is derived by stereo vision using two steps:

1. *Stereo Matching*. Given a stereo-pair image (i.e., left and right image) of an observed scene, a stereo matching model infers the so-called *disparity map*. The disparity map \mathbf{D} represents the position difference \mathbf{d} of every

²The following 3D parts of the model are obtained from external sources: Raspberry Pi HQ cameras (Inayat Rasool), Jetson Nano Devkit (Steven Minichiello), Infrared illuminator (Juan Andres Viera Medina), PIR sensor case (Mike Machado), LiPo battery (Pavel Stoudek).

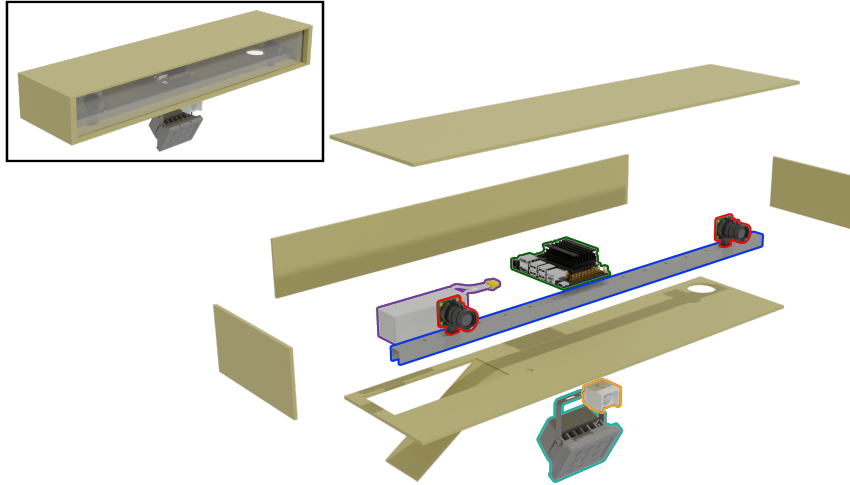


Figure 2: 3D visualization of SOCRATES. The important components will be covered in the following text and are here highlighted, i.e., cameras (red outline), baseline rail (blue outline), control unit (green outline), battery (violet outline), infrared illumination (turquoise outline), passive IR sensor (orange outline). Details such as power supply, wiring and screws are omitted. Some parts of the model are obtained from external sources².

observed scene point between the left and right image, when viewed in the right image. The disparity is inversely proportional to the distance from the stereo setup to the observed scene point depicted in the corresponding image points.³

2. *Depth Computation.* Once the disparity map is derived, the disparity values \mathbf{d} are used in combination with the so-called *extrinsic parameters* of the stereovision setup to compute the absolute depth value for each observed scene point. The extrinsic parameters are (1) the baseline b (physical distance between left and right cameras) and (2) the common focal length of both cameras f (distance between the lens and camera sensor). The absolute depth value \mathbf{z} for an observed scene point is then simply given by: $\mathbf{z} = \frac{b \cdot f}{\mathbf{d}}$. Thus, the lower the disparity, the larger the depth of the observed scene point.

2.1.2. Hardware design of SOCRATES

The SOCRATES stereovision platform is optimized for

1. operability
 - (a) at day and night time as well as
 - (b) for a wide range of animal-camera distances,

³Readers unfamiliar with this topic might use their human stereopsis by looking at a near object and a distant object alternately with only their left and right eyes, respectively. The farther object will shift less than the nearer object.

2. effective and efficient power supply,
3. hardware and construction costs,
4. weather resistance.

Cameras and Baseline: A pair of Raspberry Pi High Quality Cameras are chosen for their cost-effectiveness and the high sensitivity of their Sony IMX477 sensor (Sony Semiconductor Solutions Corporation). Interchangeable lenses allow adaptation to specific scenarios (i.e. shorter focal lengths for close-up scenes, higher focal lengths for farther away targets). Removal of the infrared filter allows sufficient exposure at night using artificial infrared illumination. The cameras have an additional Bayer filter above the sensor which we leave intact to not risk damaging the sensor itself. As near-infrared illumination (either from the environment or the illuminator) illuminates all color bands, we do not try to recover any color information and instead average all bands to obtain a grayscale image.

The cameras are mounted on a 77.5 cm long U-shaped aluminum rail with holes drilled at regular intervals to allow configuration of different baseline distances between both cameras. Both cameras are connected through 50 cm long ribbon cables to the two MIPI CSI-2 interfaces of an NVIDIA Jetson Nano Developer Kit.

Both design aspects, i.e., the interchangeable high quality lenses as well as the configurable baseline construction, allow for adaptation to specific scenarios, e.g., free fields, feeding places, animal crosses, green bridges, etc. where animals are observable at different distances.

Control: We use an NVIDIA Jetson Nano Developer Kit as the central control and storage unit. It is responsible for taking motion detection signals from the PIR sensor, turning on the power to the IR illuminator, capturing, encoding, and archiving image material from the cameras. We decided on the Jetson Nano for the following reasons: (1) compared to most single-board computers, it provides two MIPI CSI-2 interfaces for the two cameras, (2) it provides a powerful GPU that can be used for encoding video efficiently, and (3) it supports a power-efficient hibernation mode (SC7) in which it can be awakened through its general-purpose input/output (GPIO) pins by adjusting the Linux device tree accordingly. The raw RGB video material is encoded on the Jetson Nano’s GPU by synchronizing the left and right image streams, concatenating them horizontally, and compressing the resulting video of resolution $2 \times 1920 \times 1080$ using the HEVC video codec (Sullivan et al., 2012). In our experiments, this results in a bitrate of roughly 6.7Mbit/s. The Jetson Nano uses a 128GB microSDXC card for persistent storage.

Case: To make SOCRATES as weather-resistant as possible, most components are placed inside a single weather-proof case. The case is made of 0.8 cm thick birch plywood and is 80 cm wide, 11.6 cm high and 20 cm deep. We decided for a very wide case to be able to adapt the baseline of the stereo camera to different scenarios. The front of the case is shielded by a piece of acrylic glass to allow the cameras to see through. In the bottom, we add a 4 cm diameter hole for ventilation, which is covered from the inside with an insect screen. The battery

is mounted via Velcro strip onto a hatch in the bottom of the case, to allow quick replacement. We add two further holes for the wiring of the IR illuminator and motion detector, respectively, both of which are sealed using silicone. The top of the case is sealed using a silicone strip and secured by screws, which can be loosened to take it off for maintenance. All exposed wooden parts are further treated with marine varnish for weather resistance.

Motion Detection: Like most camera traps, we use a **pyroelectric infrared** (PIR) sensor for detecting motion and thereby triggering capture. We choose an HC-SR501 PIR sensor due to its compatibility with the 3.3 V GPIO pins of the Jetson Nano. We initially mounted the PIR sensor inside the case, just behind the acrylic glass. However, we found that this severely impaired the ability of the sensor to detect any kind of motion outside the case. This is because acrylic glass is opaque around wavelengths of 10 μm (Altuglas International, 2000), which corresponds to the body temperatures of most animals. Therefore, we mount the PIR sensor in a separate 3D printed weatherproof casing below the main case.

Illumination: We employ a simple 12 W, 850 nm infrared illuminator to ensure properly exposed images at night without disturbing most animals. The illuminator has a weatherproof case and is mounted on the bottom of the main case. The 12 V power supply is switched by a Jetson Nano GPIO pin using an IRLZ44NPBF MOSFET.

Power supply: All components are powered by a lithium ion polymer battery due to their high power density. We employ a battery with a theoretical capacity of 236.8 W h (16 000 mA h at 14.8 V). A generic 4S balancer circuit board provides over-discharge protection. The variable voltage of the battery is then regulated to 5 V for the Jetson Nano and 12 V for the infrared illuminator by Mean Well SCW20A-05 and SCW12A-12 converters, respectively.

Stereo correspondence: The central goal of SOCRATES is to infer depth information through stereo vision. In the natural world, as well as in computer vision, this is achieved by solving the stereo correspondence problem. Due to the different perspectives of both cameras, the same features might be located at highly different positions in both images. The stereo correspondence problem now consists of associating the same features in both images and finding their difference in position between both images. This difference is called *disparity*. The disparity is inversely proportional to the distance of the respective feature. Therefore, once the disparity is known, we have an estimation of the corresponding distance from the camera. To speed up the search for correspondences, the images from both cameras are aligned such that potential correspondences to a single feature in one image ideally lie on a single horizontal line in the other image, thereby reducing the dimensionality of the problem. This alignment is also denominated as *rectification*. To obtain an accurate rectification, the intrinsic (internal camera parameters) and extrinsic (rotation and translation between the cameras) parameters have to be obtained by a calibration procedure. For the calibration of the intrinsic parameters, a calibration object (e.g. checkerboard pattern printed on cardboard) has to be captured by the camera(s) to be able to associate 3D points in the scene with 2D points in the resulting image. To ob-

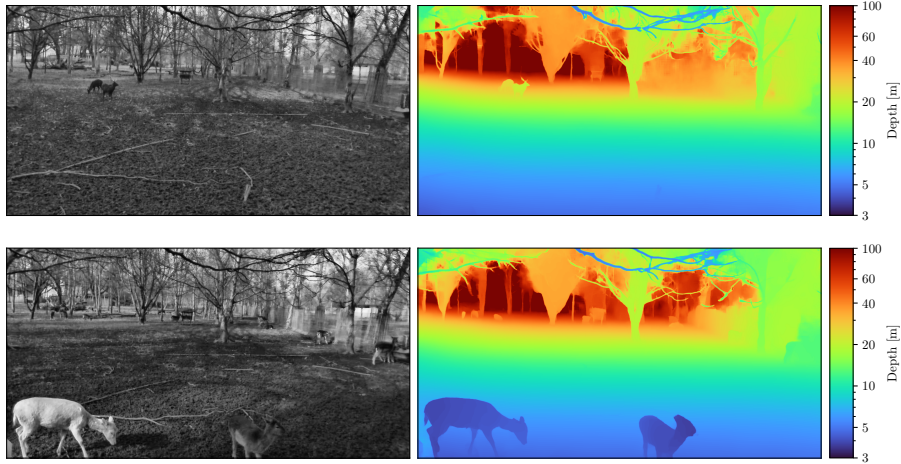


Figure 3: Samples of data collected in the *Tierpark Plittersdorf*. The left shows the grayscale image of the left camera, the right image the colorcoded depth map obtained using stereo correspondence.

tain the extrinsic parameters, eight or more correspondences between images of points in the projections of both cameras must be established (Longuet-Higgins, 1981). We perform both intrinsic and extrinsic calibration using *Kalibr* (Maye et al., 2013) with a grid of 4×3 AprilTags (Olson, 2011) mounted on a wooden board as the calibration target. During the setup of SOCRATES, the calibration target is manually moved through the scene such that it covers as much as possible of each camera’s field of view. After SOCRATES is assembled and calibrated, calibration does not have to be repeated when deployed to different locations, as the calibration is not dependent not on a specific location but only on the camera configuration. Given the intrinsic and extrinsic parameters, we rectify the images of both cameras and compute the disparity of each pixel using Li et al. (2022).

Connectivity: SOCRATES may transmit the recorded data via three different means: wired ethernet cable, wireless LAN (Edimax EW-7811UN) or cellular connection (Huawei E3372H). If no basestation is available, we use the cellular connection to manually download the captured data. Otherwise, we connect via wireless LAN and the CoAP protocol (Bormann et al., 2012) to the *AMMOD Basestation* (Wägele et al., 2022; Sixdenier et al., 2022), which in turn uploads the captured data to the *AMMOD Portal* (c.f. section 3.5).

2.2. Data

We deployed SOCRATES in the *Tierpark Plittersdorf* in order to evaluate the hardware and software. Details about this deployment may be found in section 3.1. During this time, SOCRATES made 221 true positive observations. Exemplary samples are visualized in figure 3. Each observation results in an

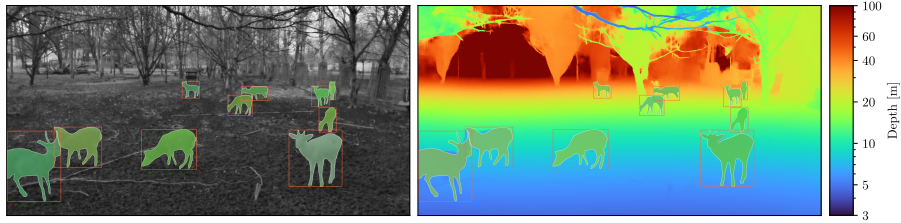


Figure 4: Examples of instance segmentation and bounding box annotations overlaid on top of the grayscale image of the left camera (left) and the color-coded depth map (right).

HEVC encoded video with 30 frames per second and a length of 25 seconds. For our experiments, we sample two sets of still images from these videos.

For abundance estimation (c.f. section 2.4), we sample still images from the videos at a rate of 2 s^{-1} , resulting in a total of 2871 images.

For the instance segmentation task (c.f. section 2.3), we want our dataset to consist of diverse scene configurations (animal positions and poses, lighting conditions, etc.). To obtain such diverse samples, sampling at regular intervals is not enough. Sometimes deer will stand still for long periods of time while moving quickly through the scene at other times. Therefore, we employ an approach based on background modeling using Gaussian mixture models (KaewTraKulPong and Bowden, 2002). We then accumulate the ratio of foreground pixels (that is, the ratio of pixels occupied by moving objects) in each video frame until a threshold of 10% is reached. This way, we sample more often if there is more movement in the video, and less often for less movement. We then annotated a total of 546 instances in 187 of the still images sampled this way with instance masks using the interactive annotation tool proposed by Sofiiuk et al. (2021). Figure 4 visualizes one such annotated image. On average, we needed roughly 3.5 minutes per instance, resulting in a total annotation effort of roughly 32 hours. Out of the total 546, we use 395 instances for training and validation (via 10-fold cross-validation), and reserve 151 instances as test dataset, such that images from a single video are only ever contained in one dataset. The test dataset is not used in this work but is instead reserved for future work. We publish both the raw data (Haucke and Steinhage, 2022b) and the instance segmentation dataset (Haucke and Steinhage, 2022a).

2.3. Depth-aware Instance Segmentation

We frame the problem of detecting and localizing animals as an instance segmentation problem, with the goal of generating a bounding box and a binary mask for each animal instance. Compared to animal presence-absence classification, this approach allows both counting the exact number of animals present, as well as inferring the distance between animal and camera by applying the binary mask to the depth images obtained using stereo vision. However, the depth images themselves obtain useful information for differentiating multiple individual animals from themselves and the background. Instance segmentation is usually

performed by first forwarding a color image with red, green and blue (RGB) channels through the backbone, which may be a convolutional neural network (CNN) or a vision transformer (Dosovitskiy et al., 2020). The backbone then generates a hierarchy of feature maps that encode higher- and higher-level information about the image. These feature maps are then used by an instance segmentation model to predict bounding boxes and binary masks themselves. It is not obvious how to use the depth images obtained from SOCRATES in this framework. Compared to datasets like ShapeNet (Chang et al., 2015), we only have information from (effectively) a single perspective. We therefore argue that it is wise to treat the depth information as an additional channel in the two-dimensional image instead of working on point clouds or voxel grids, which increase the computational and memory requirements while largely foregoing the significant improvements being made in the area of 2D instance segmentation.

Although most backbones are pre-trained on color images without depth information, one a recent work proposes *Omnivore*, a vision transformer backbone trained on color and depth information (Girdhar et al., 2022). In our experiments, we use *Omnivore* as our backbone of choice. As instance segmentation models, we use either the convolution-based *Cascade Mask R-CNN* (Cai and Vasconcelos, 2018) or the transformer-based *Mask2Former* (Cheng et al., 2022). This is motivated by the observation that vision transformers require more training data to perform well, compared to CNNs (Dosovitskiy et al., 2020; Hassani et al., 2021). Therefore, Mask2Former performs very poorly when trained on small datasets such as the *Plittersdorf instance segmentation dataset*, while outperforming Cascade Mask R-CNN on larger datasets such as Cityscapes (Cordts et al., 2016). The resulting model architecture is visualized by figure 5. To demonstrate that depth information is not only beneficial on the Plittersdorf instance segmentation task, we also evaluate improvements on the Cityscapes instance segmentation dataset. This is because the Cityscapes dataset is one of the only datasets which provides both depth information through stereo vision and a large amount of instance segmentation annotations.

We implement our instance segmentation pipeline using *mmdetection* (Chen et al., 2019) and largely keep the default hyperparameters of the mmdetection model implementations. We use the AdamW optimizer (Loshchilov and Hutter, 2017) with a global learning rate of $5N10^{-5}$ with batch size N and a weight decay of 0.05. We set $N = 2$ for Mask2Former and $N = 6$ for Cascade Mask R-CNN due to memory constraints.

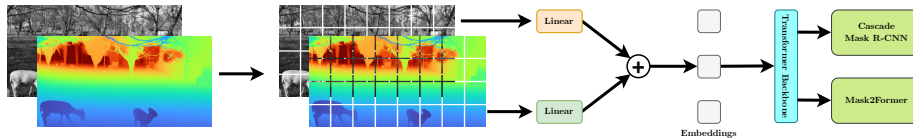


Figure 5: RGB-D Instance Segmentation using Omnivore (Girdhar et al., 2022) and Cascade Mask R-CNN (Cai and Vasconcelos, 2018) or Mask2Former (Cheng et al., 2022). In Omnivore, the grayscale and depth images are first split into 2D patches, linearly embedded and added together. The resulting embeddings are then passed through a transformer encoder which generates hierarchical feature maps. These feature maps are then used by Cascade Mask R-CNN or Mask2Former to perform instance segmentation.

2.4. Abundance Estimation using Camera Trap Distance Sampling

We may now combine the instance masks generated by the animal detection model (c.f. section 2.3) with the depth images obtained by stereo vision (c.f. section 2.1.1) to obtain the distances required for the camera trap distance sampling (CTDS, Howe et al. (2017)) abundance estimation method. To show the viability of this approach, we perform an exemplary CTDS study on the data obtained in the *Tierpark Plittersdorf*. We calculate the sampling effort according to Howe et al. (2017) as:

$$e = \frac{\theta T}{2\pi t} \quad (1)$$

where θ is the angle in radians covered by the camera trap, T is the time the camera trap was active, and t is the sample interval. For our experiment we have $\theta = 63^\circ = \frac{7\pi}{20}$, $T = 103$ d and $t = 2$ s, which results in an effort of $e = 778680$. We use 6 distance intervals from 4 m to 10 m in 1 m increments. As SOCRATES is mounted on a tree outside the compound and at a height of 1.9 m, 4 m is the minimal distance where deer are certain to be visible. Furthermore, we use the *Activity* R package (Rowcliffe et al., 2014) with a bandwidth parameter of 1 and a single replicate to estimate animal activity levels and calculate an activity rate of 0.563052. We then use the *Distance for Windows* software (Thomas et al., 2010) to estimate animal density.

3. Evaluation

3.1. SOCRATES

We operated SOCRATES in the *Tierpark Plittersdorf*, Bonn, Germany, from February 9th to July 8th 2022, or 149 days. The *Tierpark Plittersdorf* houses exclusively European fallow deer (*Dama dama*) and Sika deer (*Cervus nippon*). The camera was mounted on the side of a tree using a lashing strap and not moved during the entire duration. During this time, SOCRATES experienced temperatures from -4°C to 38°C and storms with wind speeds of 87 km h^{-1} without issues. SOCRATES was without power or the software disabled due to maintenance for 46 days, resulting in a total number of 103 observation days. During this time, SOCRATES recorded 1089 observations. Out of these, 221

	HP2XC (Reconyx)	SOCRATES
Provides Depth	✗	✓
Image Resolution	1920 × 1080 / 3MP	1920 × 1080
Video Resolution	1280 × 720	1920 × 1080
Video Length	max. 90 s at 2FPS	40 h at 30FPS
Daytime Imaging	RGB	near infrared
Nighttime Imaging	near infrared	near infrared
Dimensions	14 × 11.5 × 7.5 cm	11.6 × 80 × 20 cm
Connectivity	Cellular	Cellular / W-LAN / LAN
Battery Life	up to a year	~ 9 days
Material Cost	\$659.99	~ \$900

Table 1: Comparison between SOCRATES and the widely used Reconyx HP2XC trail camera. The video length of SOCRATES is only bounded by the available persistent storage space. Costs include only materials and not assembly.

showed visible animals. This indicates a false positive rate of roughly 80%, which is in line with prior work concerned with commercial camera traps (Newey et al., 2015). False triggers are primarily induced by (1) animals in the field-of-view of the PIR sensor, but outside of the fields of view of the cameras, (2) excessive infrared illumination by the sun during daytime or (3) by artificial light sources such as flood lights on nearby buildings. We manually removed all false positive observations from our dataset. Although this could easily be automated, e.g. by using the MegaDetector (Beery et al., 2019), we wanted to ensure that there are no persons in the final dataset and therefore screened the entire dataset manually.

We compare SOCRATES with the widely used commercially produced Reconyx HP2XC in Table 1. SOCRATES is significantly larger to support large baselines, while having significantly shorter battery life and slightly higher component costs. At the same time, SOCRATES not only provides depth information through stereo vision, but also allows recording video at high resolutions and frame rates for long durations only limited by available storage space. Approximately 80% of the triggers are false positives, which is in line with commercial trail cameras (Newey et al., 2015).

We demonstrate that the stereo capabilities SOCRATES facilitate improved visual animal detection (c.f. section 3.2) and accurate abundance estimation using camera trap distance sampling (c.f. section 3.4). Furthermore, depth information has also been shown to improve the accuracy of animal tracking over 2D-only approaches (Klasen and Steinhage, 2022a,b). SOCRATES can not compete with commercially available camera traps in cost or battery life, but this is not our goal. Apart from the methodological improvements described above, SOCRATES fulfills three high-level goals:

1. it demonstrates that stereo camera traps are viable and worthwhile. We hope to convince commercial camera trap manufacturers to support stereo camera setups using off-the-shelf hardware.

2. it facilitates the verification of monocular approaches. For example, abundance estimation using camera trap distance sampling might be performed twice, once using monocular approaches (Haucke et al., 2022; Johanns et al., 2022) and once using SOCRATES. Both raw animal distances and the resulting animal densities might then be compared.
3. it allows to generate training data for monocular depth estimation methods such as Godard et al. (2019); Ranftl et al. (2020, 2021). These approaches have been largely focused on human-centric scenes such as indoor and street scenes with relatively simple geometry, which are highly unlike natural scenes such as forests. Gathering training data from natural scenes might help these methods to generalize better to such scenes and thus allow monocular camera traps to more accurately estimate depth information in the future.

3.1.1. Stereo Correspondence

Figure 3 shows some exemplary pairs of near infrared images and corresponding depth maps inferred by (Li et al., 2022). As can be seen, the depth maps generally represent the scene well and clearly highlight the boundaries of the deer. To evaluate the depth maps quantitatively, we employ the temporal quality metric proposed in (Vandewalle and Varekamp, 2014), which is defined as:

$$E_t = \frac{1}{(N_T - 1)N_P} \sum_{n=2}^{N_T} \sum_{(x,y)} |D(x, y, n) - D(x - m_x, y - m_y, n - 1)| \quad (2)$$

where N_T is equal to the number of frames in the input video, N_P is the number of pixels in a single frame, $D(x, y, n)$ is the scalar disparity at some pixel (x, y) at time n , and m_x, m_y is the optical flow from frame n to frame $n - 1$, calculated using (Farneback, 2003). Using (Li et al., 2022), we obtain $E_t = 0.4439$, which is on-par with the temporal error of the ground truth disparity in (Vandewalle and Varekamp, 2014).

As can be seen, the temporal error is relatively low for the vast majority of observations. The median temporal error of 0.4115 is even lower than the temporal error of the ground truth disparity of Vandewalle and Varekamp (2014). Still, there are some outlier observations in which the temporal error is much worse. One such case is shown in figure 7. The depth of the well-lit area is correctly inferred, whereas poorly lit regions do not have meaningful depth information. These regions also tend to have temporally inconsistent depth values

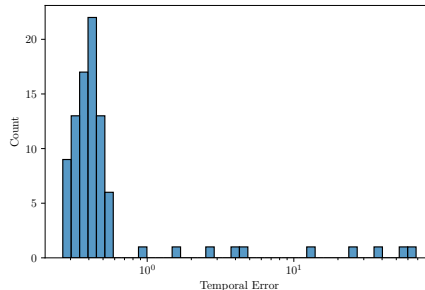


Figure 6: Histogram plot of the mean per-observation temporal stereo correspondence error.

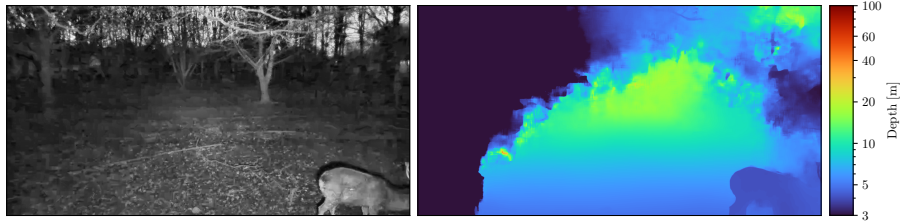


Figure 7: Stereo matching inevitably fails in regions where there is not enough available information.

Backbone	AP^{bbox}	AP_{50}^{bbox}	AP_{75}^{bbox}	AP^{segm}	AP_{50}^{segm}	AP_{75}^{segm}	AP_l^{segm}	AP_m^{segm}	AP_s^{segm}
Swin-L	0.5164	0.8438	0.5272	0.4359	0.8328	0.4285	0.5192	0.3856	0.1285
Omnivore-L	0.5243	0.8598	0.5702	0.4382	0.8353	0.4376	0.5150	0.3895	0.1431
Depth-aware Omnivore-L	0.5399	0.8494	0.6048	0.4547	0.8147	0.4699	0.5427	0.4013	0.1138

Table 2: COCO metrics on the Plittersdorf Instance Segmentation Dataset task using Cascade Mask R-CNN with different backbones and 10-fold cross-validation.

associated with them and therefore an overall high temporal error.

3.2. Visual Animal Detection

We use the COCO (Lin et al., 2014) metrics to evaluate our instance segmentation models. Each metric is obtained by performing 10-fold cross-validation after the last training epoch. Cross-validation is especially important in this setting, as it reduces the impact of a single lucky train-test split on this small dataset. Table 2 summarizes the results on the Plittersdorf instance segmentation task. The summarizing metrics for bounding boxes (AP^{bbox}) and segmentation (AP^{segm}) show that incorporating depth information results in an overall performance improvement. Interestingly, for low IOU thresholds (AP_{50}^{bbox} , AP_{50}^{segm}), depth information seems to have the opposite effect. In other words, pure grayscale images perform better for roughly localizing an animal, whereas grayscale and depth information together are better for localizing animals very accurately (AP_{75}^{bbox} , AP_{75}^{segm}). This is especially interesting as the ground truth labeling is performed using exclusively the grayscale image. Intuitively, one could therefore argue that the grayscale information is most important for matching the ground truth very precisely. Here we see the opposite effect. As the error of stereo correspondence is quadratically related to the true distance, the resulting depth maps become less useful at larger distances. This is reflected in the lower performance on small instances (AP_s^{segm}), which typically are farther away than medium (AP_m^{segm}) or large instances (AP_l^{segm}). We tried to ease the dependence on depth information for these faraway instances by clipping the depth values to different maximum distances or randomly dropping the depth information altogether during training (Srivastava et al., 2014). However, this did not result in meaningful improvements.

Backbone	AP ^{bbox}	AP ^{segm}	AP ₅₀ ^{segm}	AP _l ^{segm}	AP _m ^{segm}	AP _s ^{segm}
Swin-L		0.437	0.714			
Omnivore-L	0.415	0.439	0.700	0.716	0.394	0.214
Depth-aware Omnivore-L	0.431	0.456	0.734	0.732	0.411	0.264

Table 3: Instance segmentation results on the Cityscapes validation set. The depth-aware Omnivore-L variant clearly improves the non-depth-aware variant in all metrics. The metrics of the Swin-L backbone are obtained using the original implementation (Cheng et al., 2022). AP^{segm} and AP₅₀^{segm} are Cityscapes metrics, the rest are COCO metrics.

3.3. Depth-aware Instance Segmentation on Cityscapes

To show that the positive effect of depth information on instance segmentation accuracy is not limited to settings with grayscale images, a single object class, and a fixed camera such as SOCRATES, we additionally evaluate our instance segmentation approach on the Cityscapes instance segmentation task (Cordts et al., 2016). The Cityscapes instance segmentation dataset (Cordts et al., 2016) is composed of color and stereo depth images of urban street scenes, captured by cameras in a moving car. It features several object classes, such as *person*, *car*, or *bus*, annotated with instance labels. The Cityscapes dataset is also much larger, with 3475 annotated images in its train and validation sets. As can be seen in table 3, the depth information has an overall even greater positive impact than in the Plittersdorf task (c.f. section 3.2). This is likely caused by two reasons: (1) the Mask2Former (Cheng et al., 2022) being able to better make use of the depth-aware feature hierarchies produced by Omnivore (Girdhar et al., 2022), and (2), the larger training dataset, which might help alleviate the lower number of depth images during pre-training (Girdhar et al., 2022).

3.4. Abundance Estimation using SOCRATES

Figure 8 depicts the probability density obtained by CTDS using the parameters specified in section 2.4:

- angle θ in the observation area covered by the camera trap: $\theta = 63^\circ$,
- activity time T of camera trap: $T = 103$ days,
- time t of sample interval: $t = 2$ sec.

We visualize the probability density in figure 8. Note that the estimated probability density approximates the measurements well starting from a distance of 4 m. Due to the way SOCRATES is mounted, animals below 4 m might not be visible, which is why exclude these low distances from our estimation (c.f. section 2.4). Using the SOCRATES approach yields an estimated mean density of 8.416 ha^{-1} with a lower confidence limit of 5.360 ha^{-1} and an upper confidence limit of 13.215 ha^{-1} , given a manual estimated mean density of 11.65 ha^{-1} .

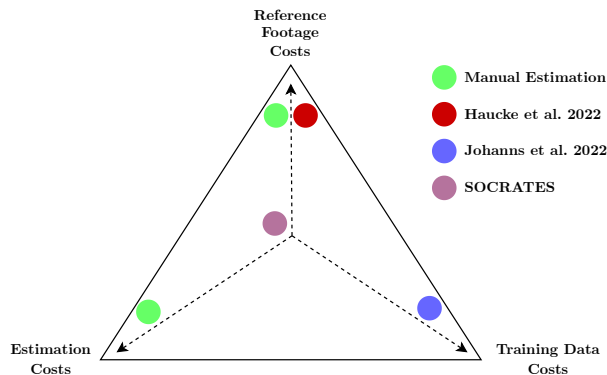


Figure 9: Tradeoff between reference footage costs, manual distance estimation costs and training data costs. The manual approach requires both the acquisition of reference footage and labour-intensive manual animal distance estimation. Haucke et al. (2022) require reference footage, but the distance estimation itself is automated. Johanns et al. (2022) require neither reference footage nor manual distance estimations, but requires training data of similar scenes. SOCRATES measures distance using stereo vision and therefore incurs none of these costs.

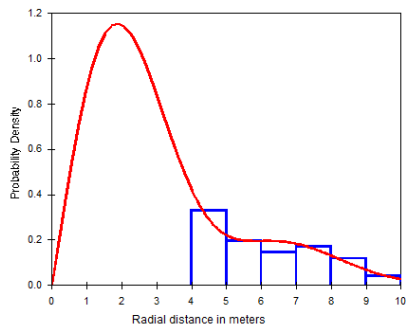


Figure 8: CTDS probability density. We transform our distance measurements into 1 m intervals (visualized in blue) from which the probability density (visualized in red) is derived using CTDS.

(2022), distance estimation for abundance estimation of unmarked animal populations is straightforward with SOCRATES. Figure 9 visualizes the respective tradeoffs.

Therefore, the proof-of-concept abundance estimation based on stereo camera trapping by SOCRATES infers animal abundance in the same order of magnitude but without any of the costs associated with competing methods (c.f. figure 9). In future studies, multiple SOCRATES installations should be used to estimate density at more sites and reduce the impact of spatially varying density. SOCRATES can also be paired cooperatively with traditional, monocular camera traps for improved error quantification and improvement of monocular distance estimations like that proposed by Johanns et al. (2022).

Compared to competing approaches (Haucke et al., 2022; Johanns et al.,

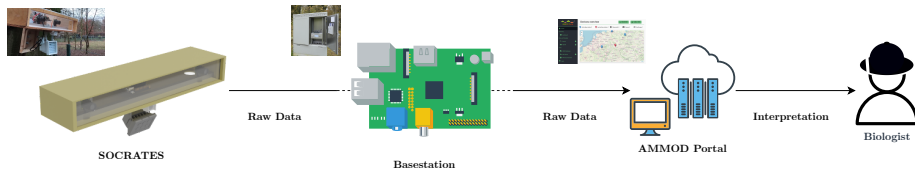


Figure 10: Fully automatic flow of data from SOCRATES over the basestation to the AMMOD Portal and the expert end users. A GPU server runs the instance segmentation and distance estimation steps, and uploads the results back to the AMMOD portal.

3.5. AMMOD Portal Case Study

A central goal of the AMMOD project is to automatically collect all observed data in a central repository (the *AMMOD Portal*, <https://data.ammod.de>), which will eventually be accessible to biologists and the general public. For SOCRATES, we ensure this by uploading the captured raw data via the CoAP protocol (Bormann et al., 2012) to the *AMMOD Basestation* (Wägele et al., 2022; Sixdenier et al., 2022), if available at the current location, or directly to the AMMOD Portal otherwise. The AMMOD Basestation takes the role of scheduling and prioritizing data transfer from different sensors according to the energy available from energy harvesting. Once the raw data is uploaded to the AMMOD Portal, a server runs the instance segmentation (cf. section 2.3) and distance estimation (c.f. section 2.4) workflows. To increase throughput and energy efficiency, the server is equipped with an NVIDIA GPU to accelerate neural network inference. Both methods are packaged as *Docker* images to simplify dependency management and updates. The resulting instance masks and distances are then again uploaded to the AMMOD Portal and are available for further analysis by biologists. The entire data flow is fully automated and visualized in figure 10.

4. Conclusion

We propose a **StereO CameRA Trap** for monitoring of biodiversity (SOCRATES), a novel camera trap prototype that uses stereo vision to infer the 3D structure of the captured scene. SOCRATES enables the following contributions:

- **Detection and localization of animals:** SOCRATES provides depth information that improves the accurate localization of animals in an instance segmentation setting, e.g. by 3.23% in bounding box mAP₇₅. We obtain these results by performing 10-fold cross-validation. Similar results on the Cityscapes instance segmentation task show that this effect is neither limited to grayscale images, a single object category, nor fixed cameras such as SOCRATES.
- **Abundance estimation** is facilitated by the automatic distance measurements of SOCRATES. We perform a proof-of-concept camera trap distance sampling study and estimate accurate animal density estimates for a zoo scenario. Future work might use SOCRATES to perform automatic abundance estimation in the wild and compare the results with competing approaches.
- **Reproducibility and accessibility** for practitioners is enabled by openly providing our raw and labeled data, code, detailed instructions, best practices, and 3D CAD models at <https://github.com/timmh/socrates>. We hope to pave the way for the eventual adaption of stereo camera traps by commercial manufacturers.

References

- Altuglas International, 2000. Plexiglas – optical & transmission characteristics. Arkema, Philadelphia, PA .
- Auda, E., 2022. Overestimation of animal distances in close-up scenarios. Wildlife Conservation Society - Cambodia. Personal communication.
- Beery, S., Morris, D., Yang, S., 2019. Efficient pipeline for camera trap image review. arXiv preprint arXiv:1907.06772 .
- Bormann, C., Castellani, A.P., Shelby, Z., 2012. Coap: An application protocol for billions of tiny internet nodes. *IEEE Internet Computing* 16, 62–67. doi:10.1109/MIC.2012.29.
- Cai, Z., Vasconcelos, N., 2018. Cascade r-cnn: Delving into high quality object detection, in: *Proceedings of the IEEE conference on computer vision and pattern recognition*, pp. 6154–6162.
- Chang, A.X., Funkhouser, T., Guibas, L., Hanrahan, P., Huang, Q., Li, Z., Savarese, S., Savva, M., Song, S., Su, H., Xiao, J., Yi, L., Yu, F., 2015. ShapeNet: An Information-Rich 3D Model Repository. Technical Report arXiv:1512.03012 [cs.GR]. Stanford University — Princeton University — Toyota Technological Institute at Chicago.
- Chen, K., Wang, J., Pang, J., Cao, Y., Xiong, Y., Li, X., Sun, S., Feng, W., Liu, Z., Xu, J., Zhang, Z., Cheng, D., Zhu, C., Cheng, T., Zhao, Q., Li, B., Lu, X., Zhu, R., Wu, Y., Dai, J., Wang, J., Shi, J., Ouyang, W., Loy, C.C., Lin, D., 2019. MMDetection: Open mmlab detection toolbox and benchmark. arXiv preprint arXiv:1906.07155 .
- Cheng, B., Misra, I., Schwing, A.G., Kirillov, A., Girdhar, R., 2022. Masked-attention mask transformer for universal image segmentation.
- Cordts, M., Omran, M., Ramos, S., Rehfeld, T., Enzweiler, M., Benenson, R., Franke, U., Roth, S., Schiele, B., 2016. The cityscapes dataset for semantic urban scene understanding, in: *Proceedings of the IEEE Conference on Computer Vision and Pattern Recognition (CVPR)*.
- Deng, J., Dong, W., Socher, R., Li, L.J., Li, K., Fei-Fei, L., 2009. ImageNet: A Large-Scale Hierarchical Image Database, in: *CVPR09*.
- Dosovitskiy, A., Beyer, L., Kolesnikov, A., Weissenborn, D., Zhai, X., Unterthiner, T., Dehghani, M., Minderer, M., Heigold, G., Gelly, S., et al., 2020. An image is worth 16x16 words: Transformers for image recognition at scale. arXiv preprint arXiv:2010.11929 .
- Farnebäck, G., 2003. Two-frame motion estimation based on polynomial expansion, in: *Scandinavian conference on Image analysis*, Springer. pp. 363–370.

- Girdhar, R., Singh, M., Ravi, N., van der Maaten, L., Joulin, A., Misra, I., 2022. Omnivore: A Single Model for Many Visual Modalities, in: CVPR.
- Godard, C., Mac Aodha, O., Firman, M., Brostow, G.J., 2019. Digging into self-supervised monocular depth prediction .
- Hassani, A., Walton, S., Shah, N., Abuduweili, A., Li, J., Shi, H., 2021. Escaping the big data paradigm with compact transformers. CoRR abs/2104.05704. URL: <https://arxiv.org/abs/2104.05704>, arXiv:2104.05704.
- Haucke, T., Köhl, H.S., Hoyer, J., Steinhage, V., 2022. Overcoming the distance estimation bottleneck in estimating animal abundance with camera traps. *Ecological Informatics* 68, 101536. URL: <https://www.sciencedirect.com/science/article/pii/S1574954121003277>, doi:<https://doi.org/10.1016/j.ecoinf.2021.101536>.
- Haucke, T., Steinhage, V., 2022a. SOCRATES Plittersdorf Instance Segmentation Dataset. URL: <https://doi.org/10.5281/zenodo.7035934>, doi:10.5281/zenodo.7035934.
- Haucke, T., Steinhage, V., 2022b. SOCRATES Plittersdorf Raw Data. URL: <https://doi.org/10.5281/zenodo.6992653>, doi:10.5281/zenodo.6992653.
- Howe, E.J., Buckland, S.T., Després-Einspenner, M.L., Köhl, H.S., 2017. Distance sampling with camera traps. *Methods in Ecology and Evolution* 8, 1558–1565. URL: <https://besjournals.onlinelibrary.wiley.com/doi/abs/10.1111/2041-210X.12790>, doi:10.1111/2041-210X.12790, arXiv:<https://besjournals.onlinelibrary.wiley.com/doi/pdf/10.1111/2041-210X.12790>.
- Inayat Rasool, . Raspberry pi hq camera with arducam cs mount lens. <https://grabcad.com/library/raspberry-pi-hq-camera-with-arducam-cs-mount-lens-1>.
- Johanns, P., Haucke, T., Steinhage, V., 2022. Automated distance estimation for wildlife camera trapping. *Ecological Informatics* 70, 101734. URL: <https://www.sciencedirect.com/science/article/pii/S1574954122001844>, doi:<https://doi.org/10.1016/j.ecoinf.2022.101734>.
- Juan Andres Viera Medina, . Infrared illuminator. <https://grabcad.com/library/infrared-illuminator-1>.
- KaewTraKulPong, P., Bowden, R., 2002. An improved adaptive background mixture model for real-time tracking with shadow detection, in: Video-based surveillance systems. Springer, pp. 135–144.
- Klasen, M., Steinhage, V., 2022a. Improving wildlife tracking using 3d information. *Ecological Informatics* 68, 101535. URL: <https://www.sciencedirect.com/science/article/pii/S1574954121003265>, doi:<https://doi.org/10.1016/j.ecoinf.2021.101535>.

- Klasen, M., Steinhage, V., 2022b. Wildlife 3d multi-object tracking. *Ecological Informatics* 71, 101790. URL: <https://www.sciencedirect.com/science/article/pii/S1574954122002400>, doi:<https://doi.org/10.1016/j.ecoinf.2022.101790>.
- Li, J., Wang, P., Xiong, P., Cai, T., Yan, Z., Yang, L., Liu, J., Fan, H., Liu, S., 2022. Practical stereo matching via cascaded recurrent network with adaptive correlation, in: *Proceedings of the IEEE/CVF Conference on Computer Vision and Pattern Recognition*, pp. 16263–16272.
- Lin, T., Maire, M., Belongie, S.J., Bourdev, L.D., Girshick, R.B., Hays, J., Perona, P., Ramanan, D., Dollár, P., Zitnick, C.L., 2014. Microsoft COCO: common objects in context. CoRR abs/1405.0312. URL: <http://arxiv.org/abs/1405.0312>, arXiv:1405.0312.
- Longuet-Higgins, H.C., 1981. A computer algorithm for reconstructing a scene from two projections. *Nature* 293, 133–135.
- Loshchilov, I., Hutter, F., 2017. Fixing weight decay regularization in adam. CoRR abs/1711.05101. URL: <http://arxiv.org/abs/1711.05101>, arXiv:1711.05101.
- Maye, J., Furgale, P., Siegwart, R., 2013. Self-supervised calibration for robotic systems, in: *2013 IEEE Intelligent Vehicles Symposium (IV)*, IEEE. pp. 473–480.
- Mike Machado, . Pir sensor wall mount enclosure. <https://www.thingiverse.com/thing:1718985>. This work is licensed under the Creative Commons Attribution 4.0 International License. To view a copy of this license, visit <http://creativecommons.org/licenses/by/4.0/>.
- Moeller, A.K., Lukacs, P.M., Horne, J.S., 2018. Three novel methods to estimate abundance of unmarked animals using remote cameras. *Ecosphere* 9, e02331.
- Nakashima, Y., Fukasawa, K., Samejima, H., 2018. Estimating animal density without individual recognition using information derivable exclusively from camera traps. *Journal of Applied Ecology* 55, 735–744.
- Newey, S., Davidson, P., Nazir, S., Fairhurst, G., Verdicchio, F., Irvine, R.J., van der Wal, R., 2015. Limitations of recreational camera traps for wildlife management and conservation research: A practitioner’s perspective. *Ambio* 44, 624–635.
- Olson, E., 2011. Apriltag: A robust and flexible visual fiducial system, in: *2011 IEEE international conference on robotics and automation*, IEEE. pp. 3400–3407.
- Pavel Stoudek, . Tattu 4s 6750mah lipo battery. <https://grabcad.com/library/tattu-4s-6750mah-lipo-battery-1>.

- Ranftl, R., Bochkovskiy, A., Koltun, V., 2021. Vision transformers for dense prediction. arXiv preprint arXiv:2103.13413 .
- Ranftl, R., Lasinger, K., Hafner, D., Schindler, K., Koltun, V., 2020. Towards robust monocular depth estimation: Mixing datasets for zero-shot cross-dataset transfer. *IEEE Transactions on Pattern Analysis and Machine Intelligence (TPAMI)* .
- Reconyx, . Hp2xc hyperfire 2 cellular professional covert ir camera. <https://www.reconyx.com/product/hyperfire-2-cellular-professional-covert-ir-camera>.
- Rowcliffe, J.M., Field, J., Turvey, S.T., Carbone, C., 2008. Estimating animal density using camera traps without the need for individual recognition. *Journal of Applied Ecology* 45, 1228–1236.
- Rowcliffe, J.M., Kays, R., Kranstauber, B., Carbone, C., Jansen, P.A., 2014. Quantifying levels of animal activity using camera trap data. *Methods in Ecology and Evolution* 5, 1170–1179. URL: <https://besjournals.onlinelibrary.wiley.com/doi/abs/10.1111/2041-210X.12278>, doi:<https://doi.org/10.1111/2041-210X.12278>, arXiv:<https://besjournals.onlinelibrary.wiley.com/doi/pdf/10.1111/2041-210X.12278>.
- Sixdenier, P.L., Wildermann, S., Ziegler, D., Teich, J., 2022. Sidam: A design space exploration framework for multi-sensor embedded systems powered by energy harvesting, in: Orailoglu, A., Reichenbach, M., Jung, M. (Eds.), *Embedded Computer Systems: Architectures, Modeling, and Simulation*, Springer International Publishing, Cham. pp. 329–345.
- Sofiuk, K., Petrov, I.A., Konushin, A., 2021. Reviving iterative training with mask guidance for interactive segmentation. arXiv preprint arXiv:2102.06583 .
- Sony Semiconductor Solutions Corporation, . Imx477-aack product information. https://www.sony-semicon.co.jp/products/common/pdf/IMX477-AACK_Flyer.pdf.
- Srivastava, N., Hinton, G., Krizhevsky, A., Sutskever, I., Salakhutdinov, R., 2014. Dropout: a simple way to prevent neural networks from overfitting. *The journal of machine learning research* 15, 1929–1958.
- Steven Minichiello, . nvidia jetson nano development board. <https://grabcad.com/library/nvidia-jetson-nano-development-board-1>.
- Sullivan, G.J., Ohm, J.R., Han, W.J., Wiegand, T., 2012. Overview of the high efficiency video coding (hevc) standard. *IEEE Transactions on Circuits and Systems for Video Technology* 22, 1649–1668. doi:10.1109/TCSVT.2012.2221191.

- Thomas, L., Buckland, S.T., Rexstad, E.A., Laake, J.L., Strindberg, S., Hedley, S.L., Bishop, J.R., Marques, T.A., Burnham, K.P., 2010. Distance software: design and analysis of distance sampling surveys for estimating population size. *Journal of Applied Ecology* 47, 5–14. URL: <https://besjournals.onlinelibrary.wiley.com/doi/abs/10.1111/j.1365-2664.2009.01737.x>, doi:<https://doi.org/10.1111/j.1365-2664.2009.01737.x>, arXiv:<https://besjournals.onlinelibrary.wiley.com/doi/pdf/10.1111/j.1365-2664.2009.01737.x>
- Vandewalle, P., Varekamp, C., 2014. Disparity map quality for image-based rendering based on multiple metrics, in: 2014 International Conference on 3D Imaging (IC3D), IEEE. pp. 1–5.
- Wägele, J., Bodesheim, P., Bourlat, S.J., Denzler, J., Diepenbroek, M., Fonseca, V., Frommolt, K.H., Geiger, M.F., Gemeinholzer, B., Glöckner, F.O., Haucke, T., Kirse, A., Kölpin, A., Kostadinov, I., Köhl, H.S., Kurth, F., Lasseck, M., Liedke, S., Losch, F., Müller, S., Petrovskaya, N., Piotrowski, K., Radig, B., Scherber, C., Schoppmann, L., Schulz, J., Steinhage, V., Tschan, G.F., Vautz, W., Velotto, D., Weigend, M., Wildermann, S., 2022. Towards a multisensor station for automated biodiversity monitoring. *Basic and Applied Ecology* 59, 105–138. URL: <https://www.sciencedirect.com/science/article/pii/S1439179122000032>, doi:<https://doi.org/10.1016/j.baae.2022.01.003>.
- Zeiler, M.D., Fergus, R., 2014. Visualizing and understanding convolutional networks, in: European conference on computer vision, Springer. pp. 818–833.